Supplementary Information (SI) for Sustainable Energy & Fuels.

Electronic Supporting Information File for;

A Porphyrin Polyethylenimine Polymer as an Effective Photosensitiser for Hydrogen Evolution

P. Loftus, L. Tabrizi, M. P. Brandon, and M. T. Pryce

School of Chemical Sciences, Dublin City University, Glasnevin, Dublin, D09 V289, Ireland.

Contents

S1. Synthesis and Characterisation

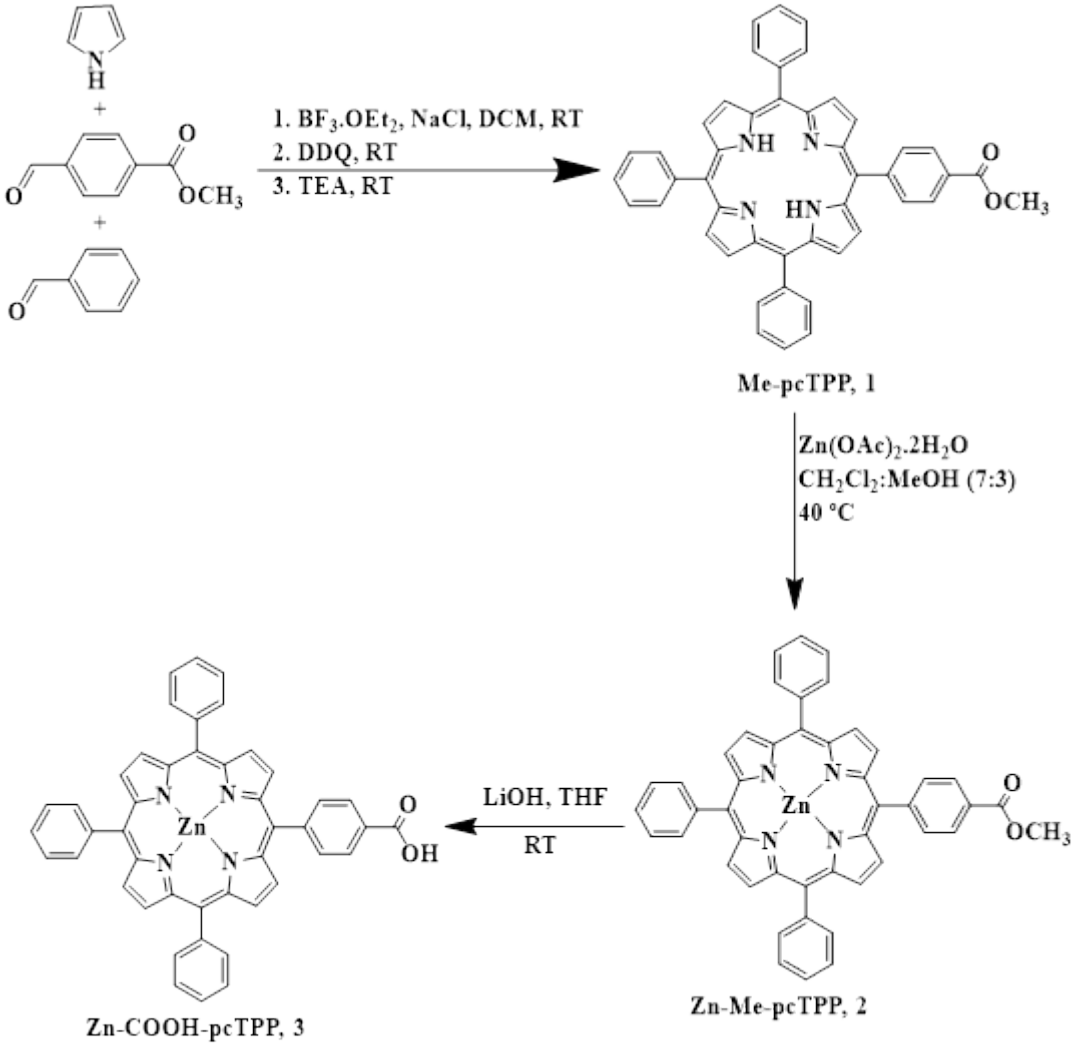

Scheme S1: Synthetic approach for the synthesis of Zn-COOH-pcTPP,

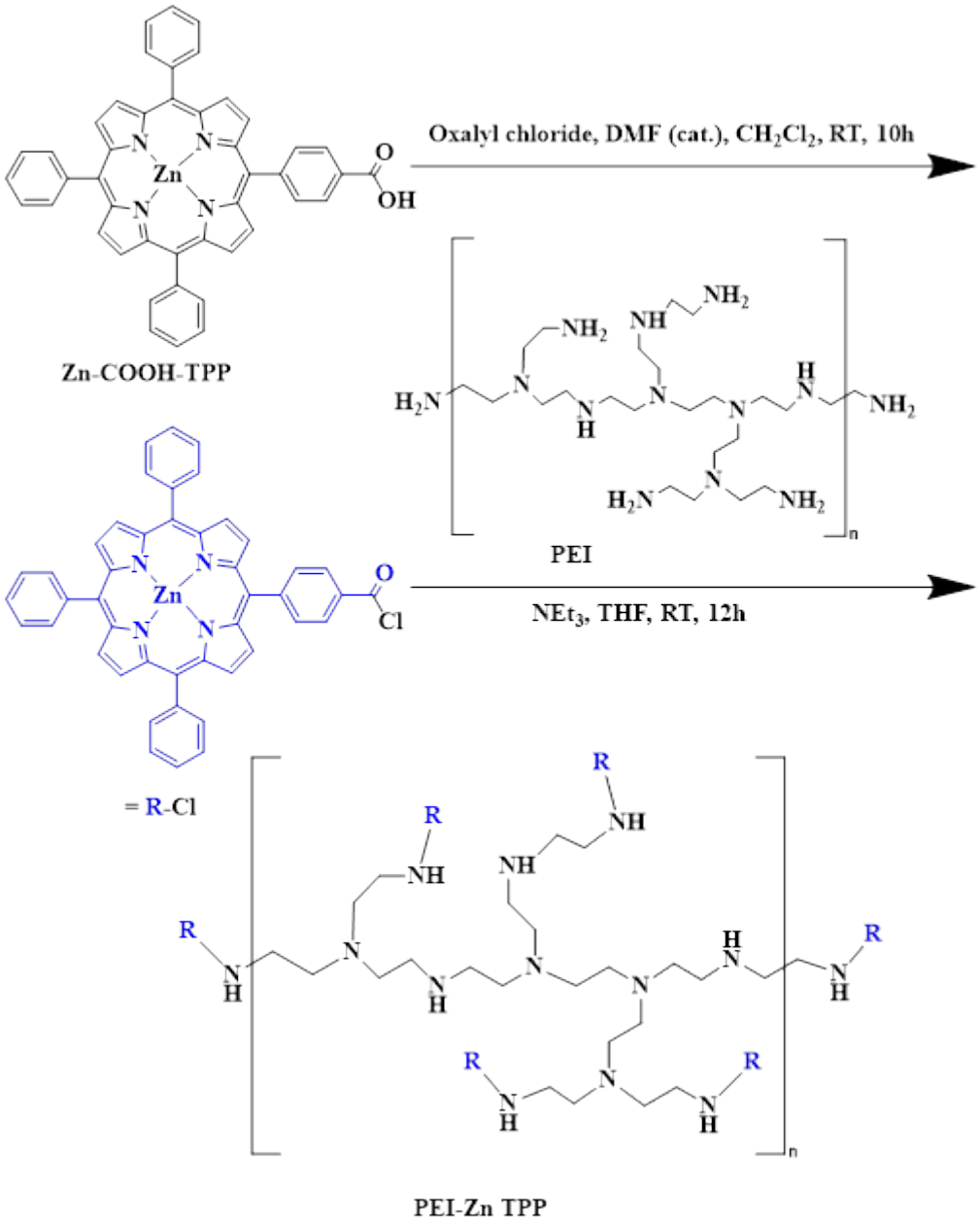

Scheme S2: Synthetic approach for the final PEI-ZnTPP polymer

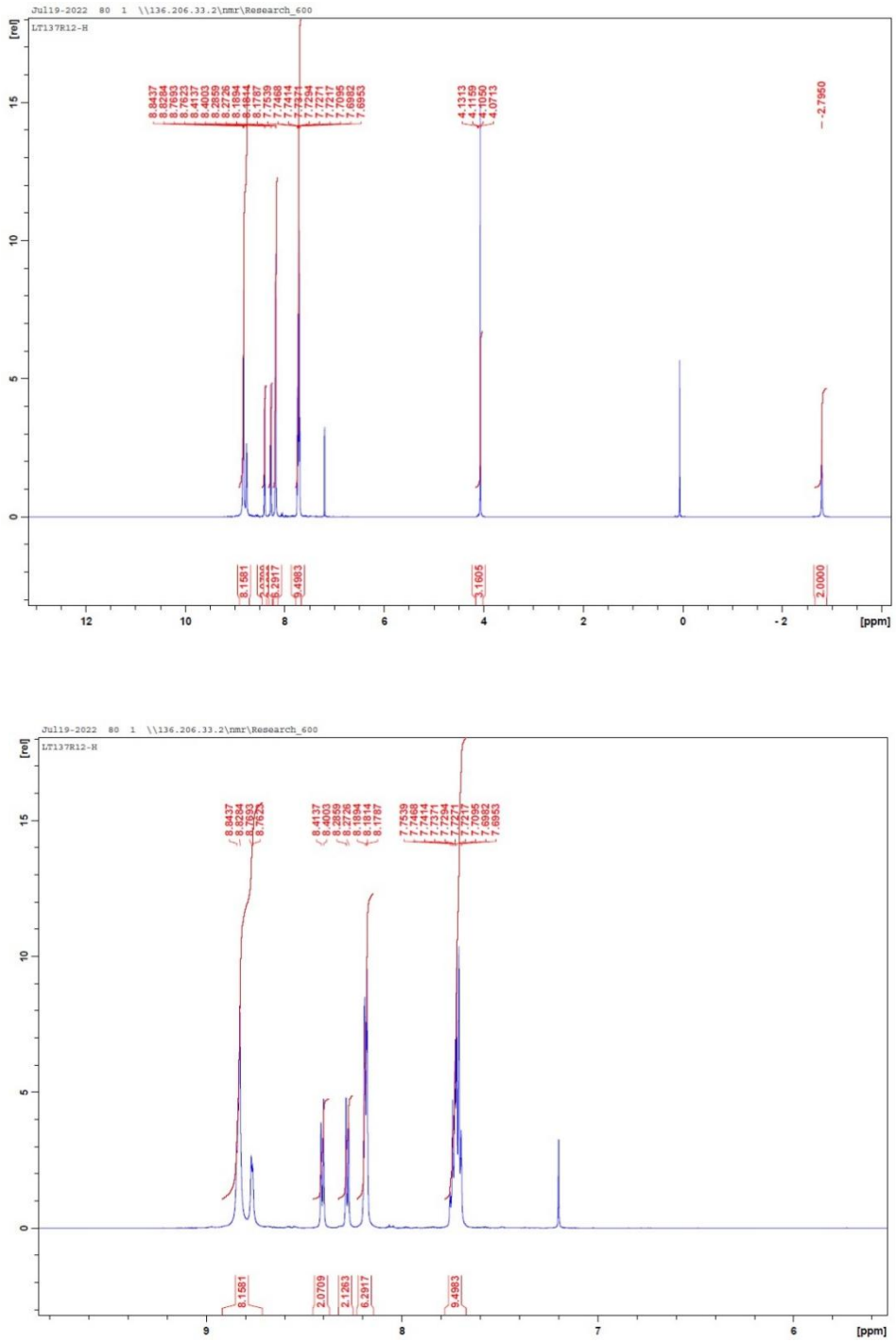

Fig. S1: ^{1}HNMR spectrum of Me-pcTPP in $CDCl_3$

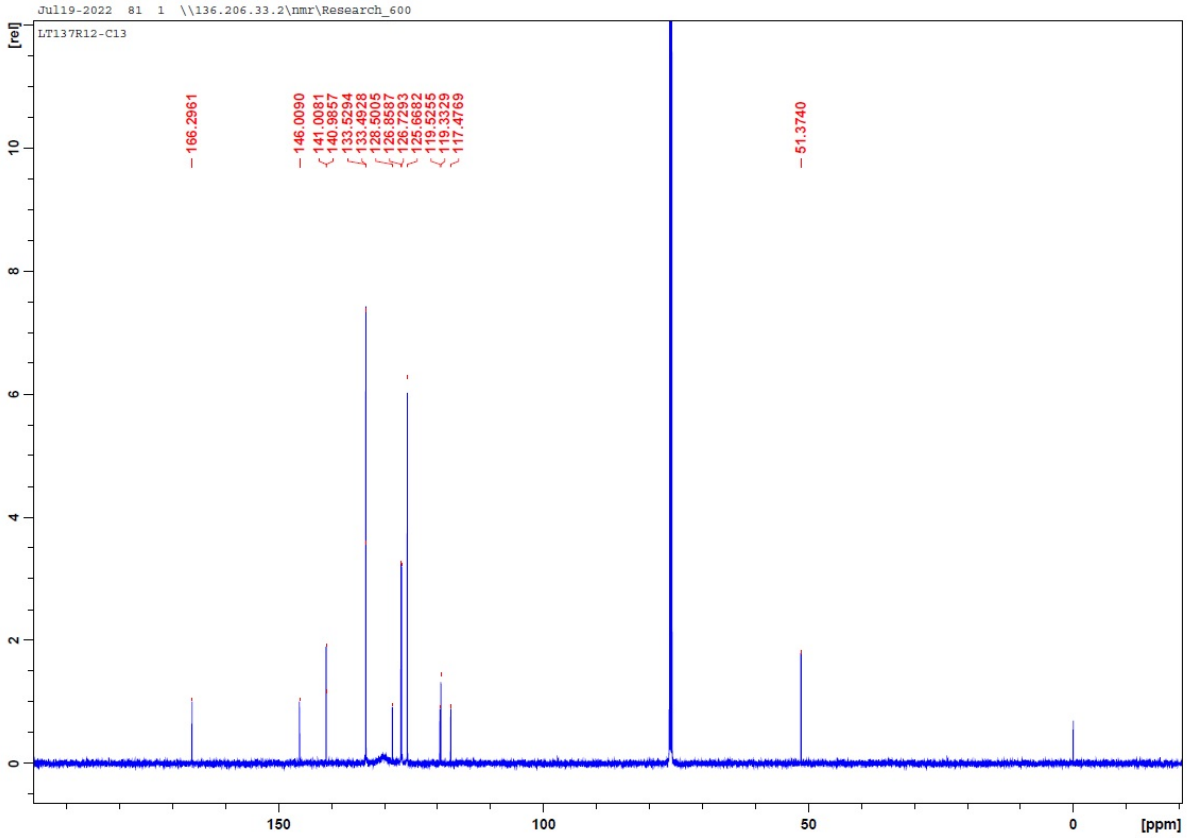

Fig. S2: ^{13}CNMR spectrum of Me-pcTPP in $CDCl_3$

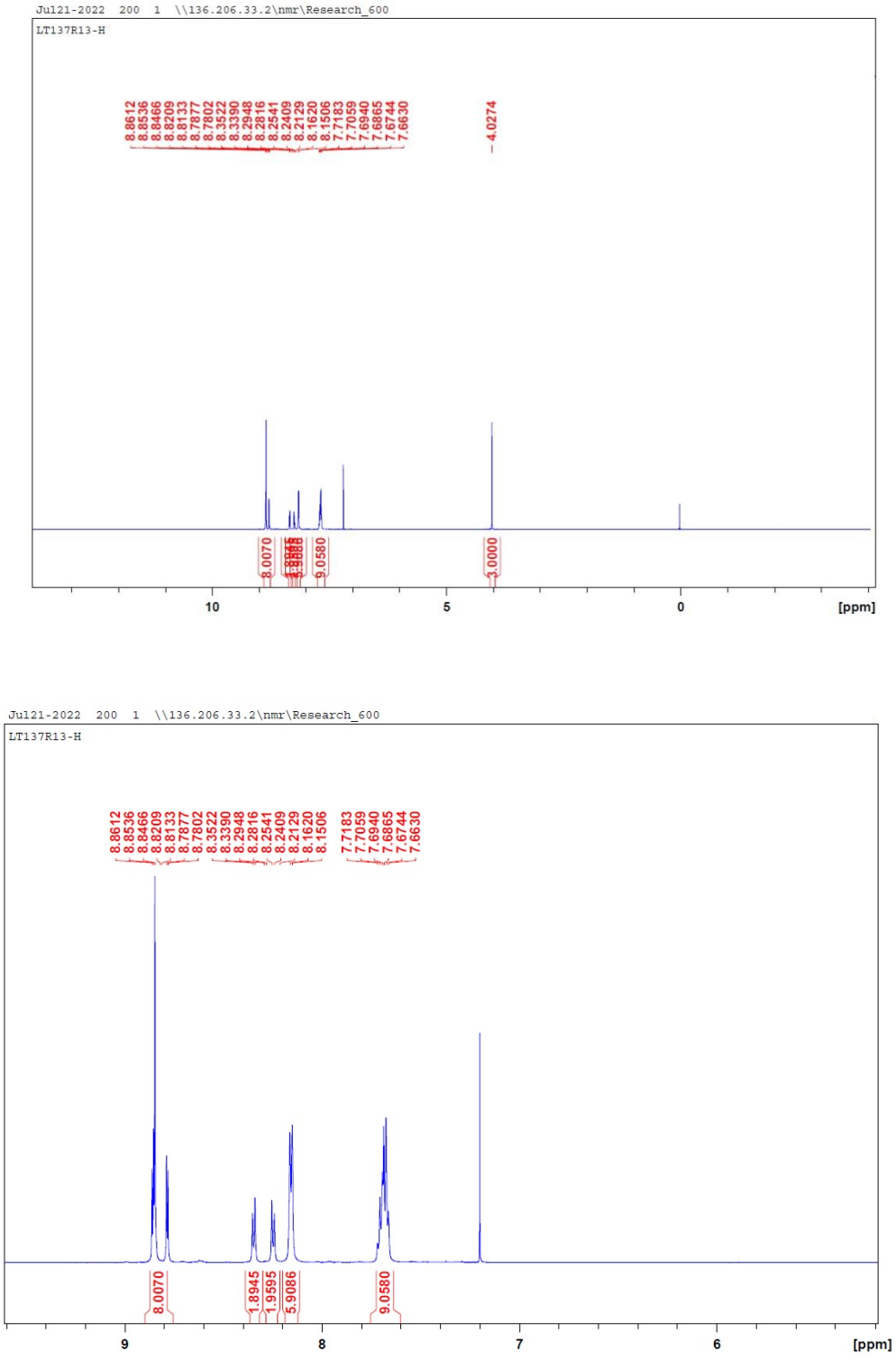

Fig. S3: ^{1}HNMR spectrum of Zn-Me-pcTPP, **2** in $CDCl_3$.

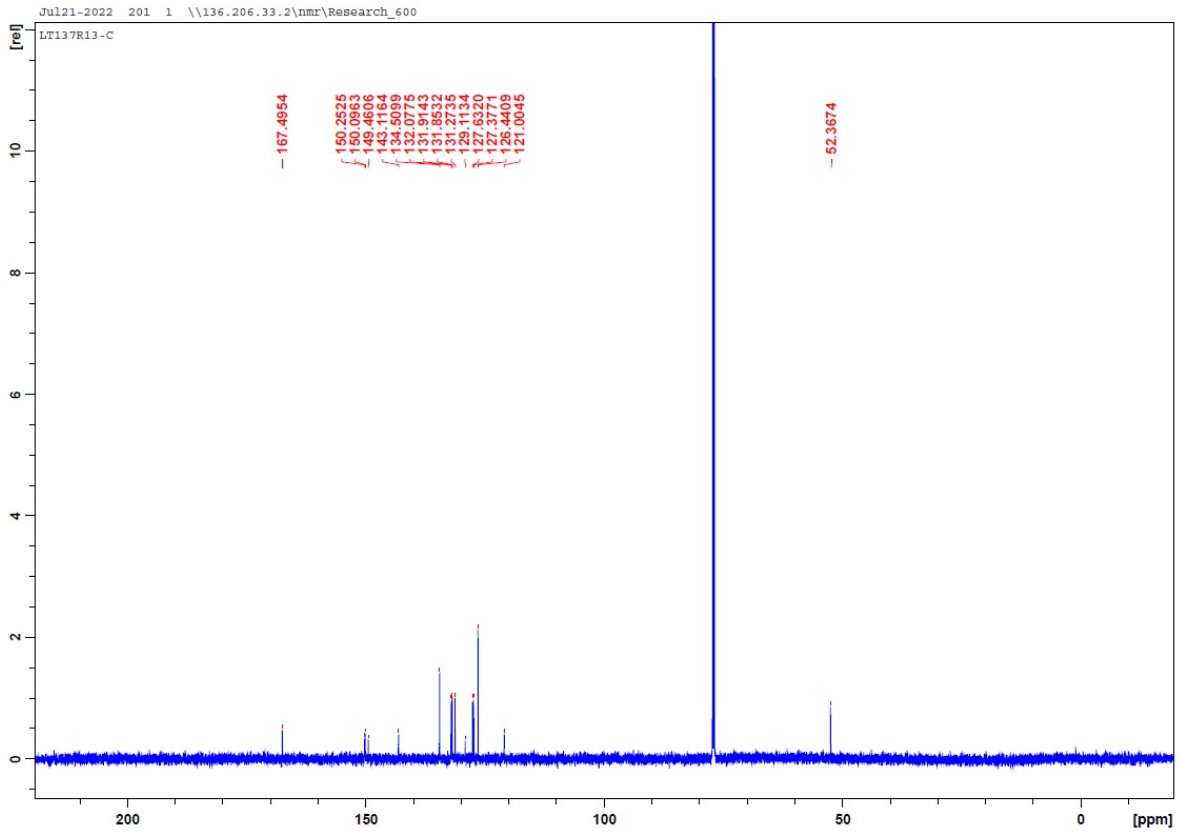

Fig. S4: ^{13}CNMR spectrum of Zn-Me-pcTPP, **2** in $CDCl_3$.

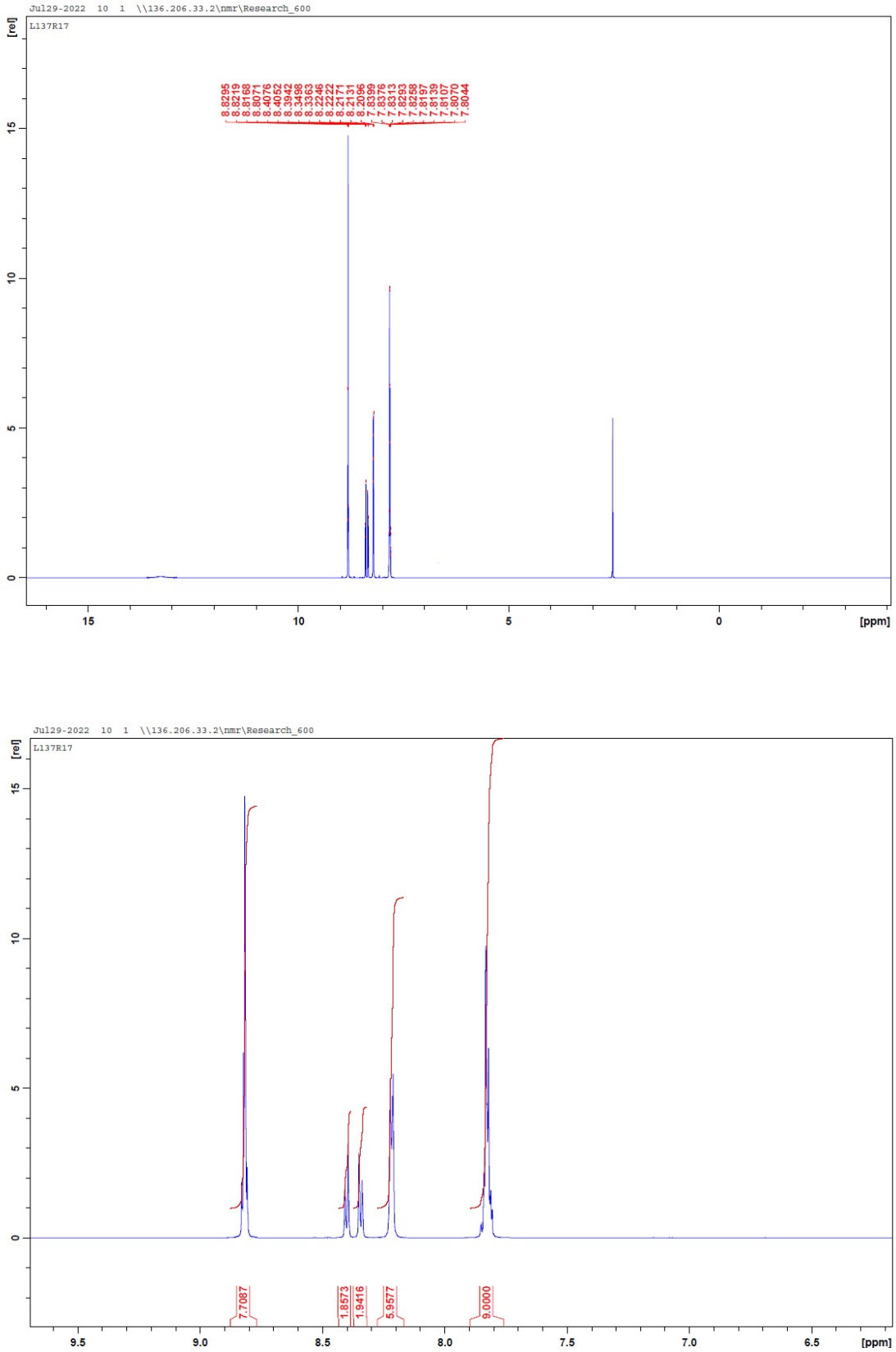

Fig. S5: ^{1}H NMR spectrum of (Zn-COOH-TPP), 3 in DMSO-d_6.

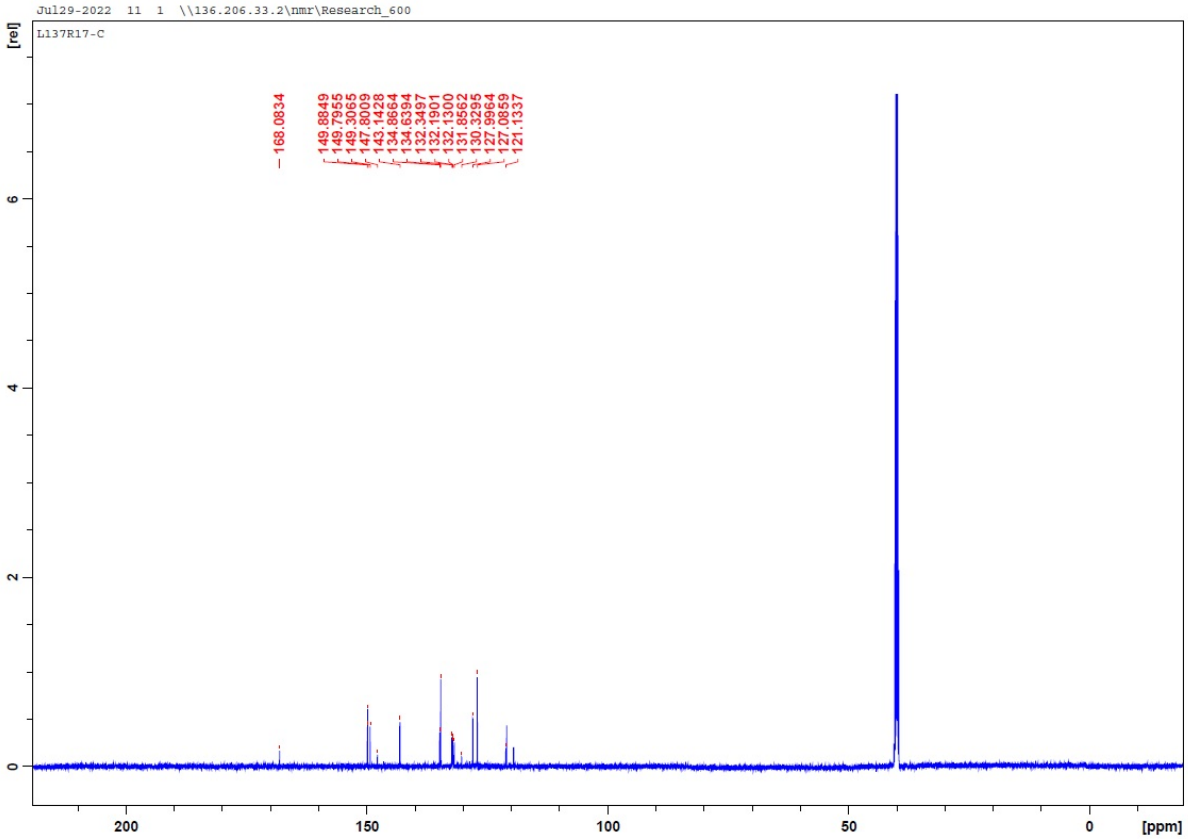

Fig. S6: ^{13}C NMR spectrum of (Zn-COOH-TPP), 3 in DMSO-d_6.

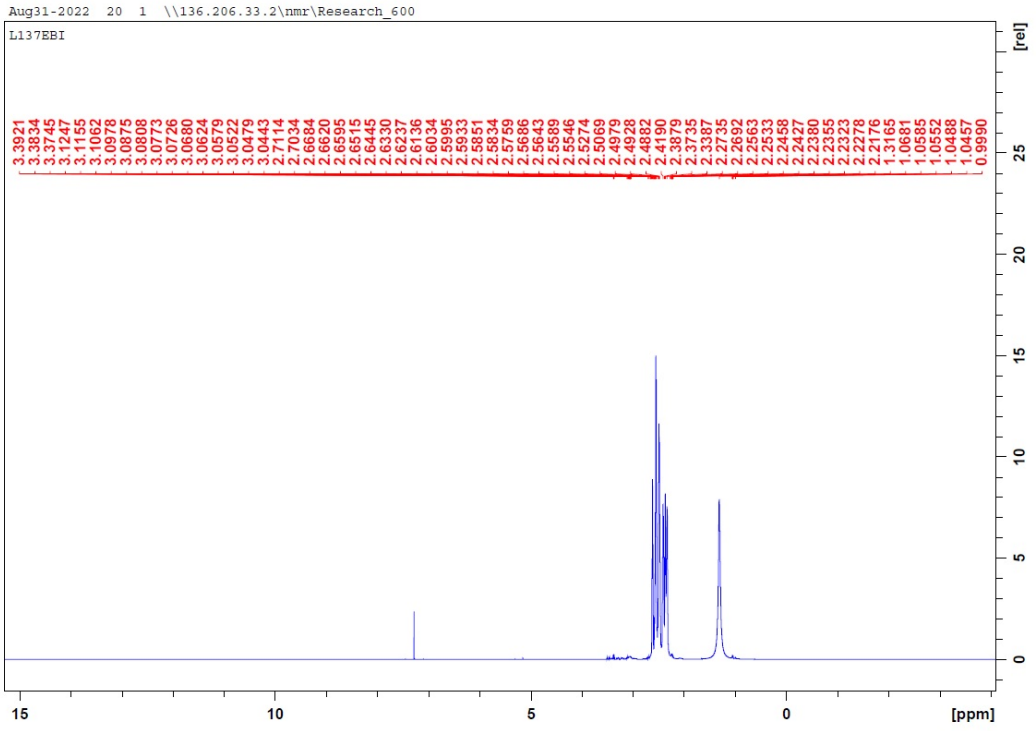

Fig. S7: ^{1}H NMR spectrum of PEI polymer in $CDCl_3$.

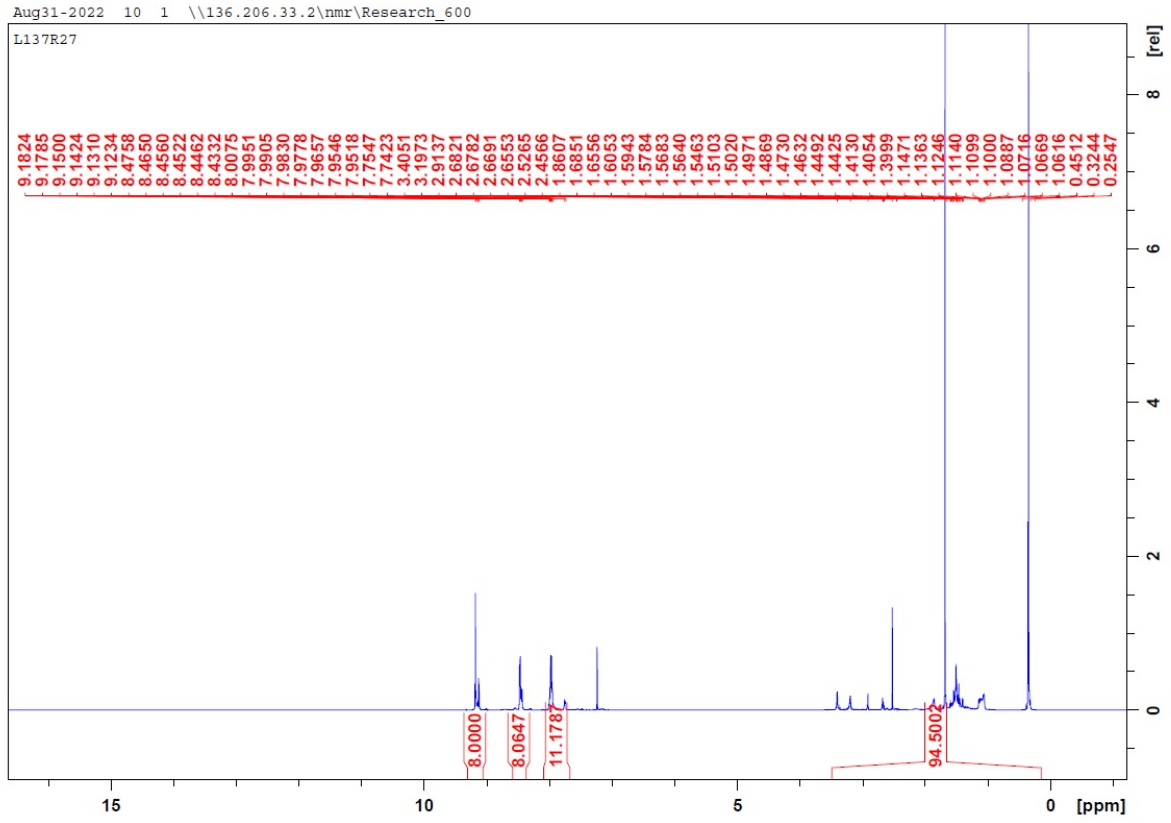

Fig. S8: ^{1}H NMR spectrum of PEI-Zn TPP polymer in $CDCl_3$.

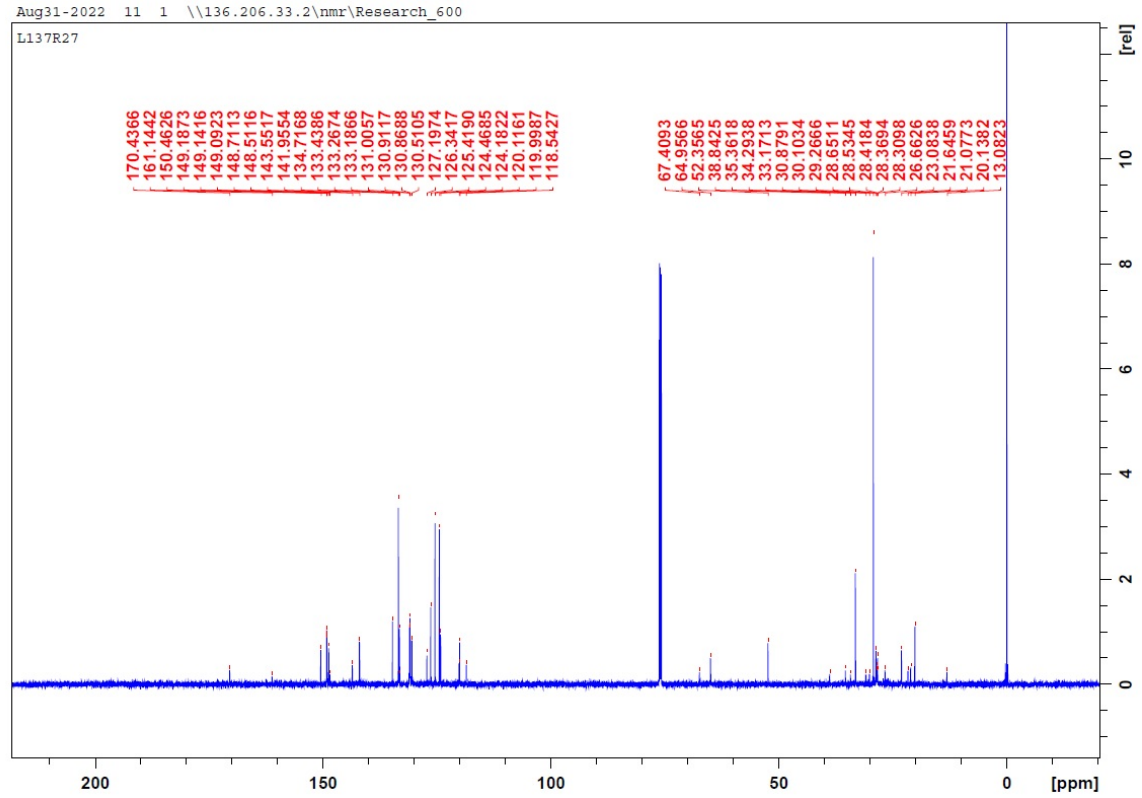

Fig. S9: ^{13}C NMR spectrum of PEI-Zn TPP polymer in $CDCl_3$.

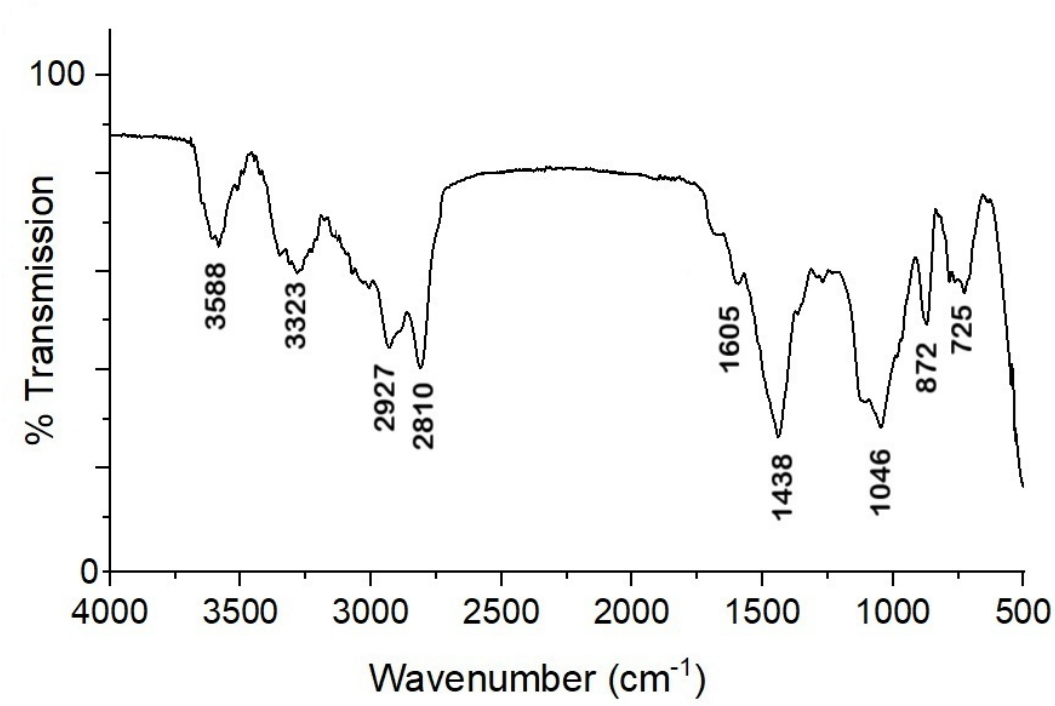

Fig. S10: FT-IR spectrum of PEI polymer

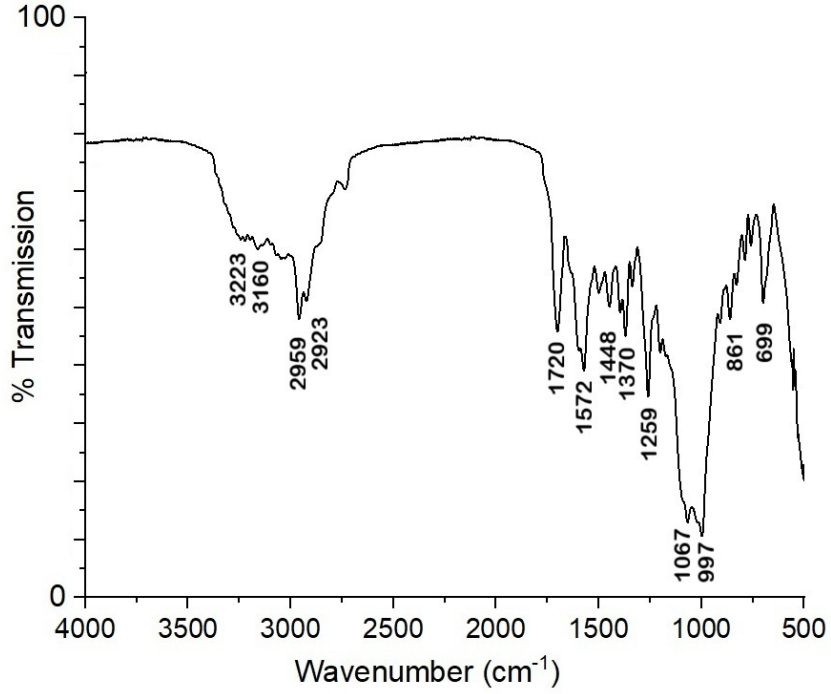

Fig. S11: FT-IR spectrum of PEI-Zn TPP polymer

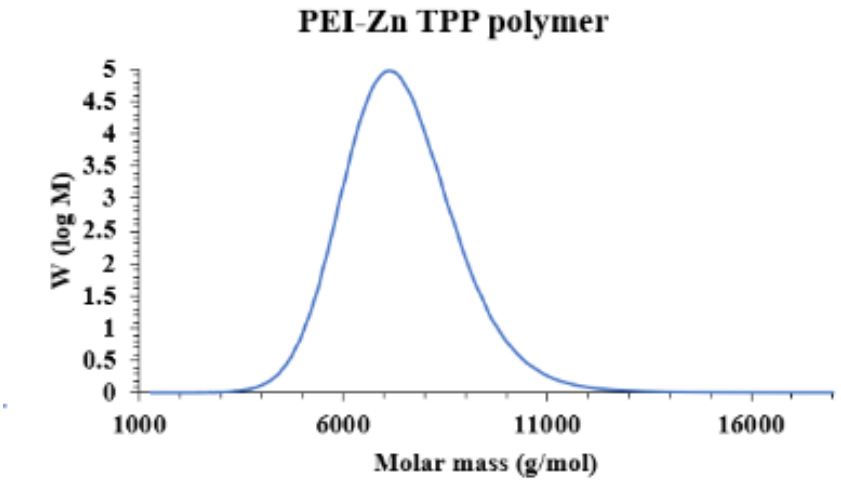

Fig. S12: GPC RI traces of PEI-ZnTPP polymer

Table S1: GPC results of PEI-ZnTPP polymer

M_n	M_w	M_p	D_M
6900 g/mol	7164 g/mol	7167 g/mol	1.04

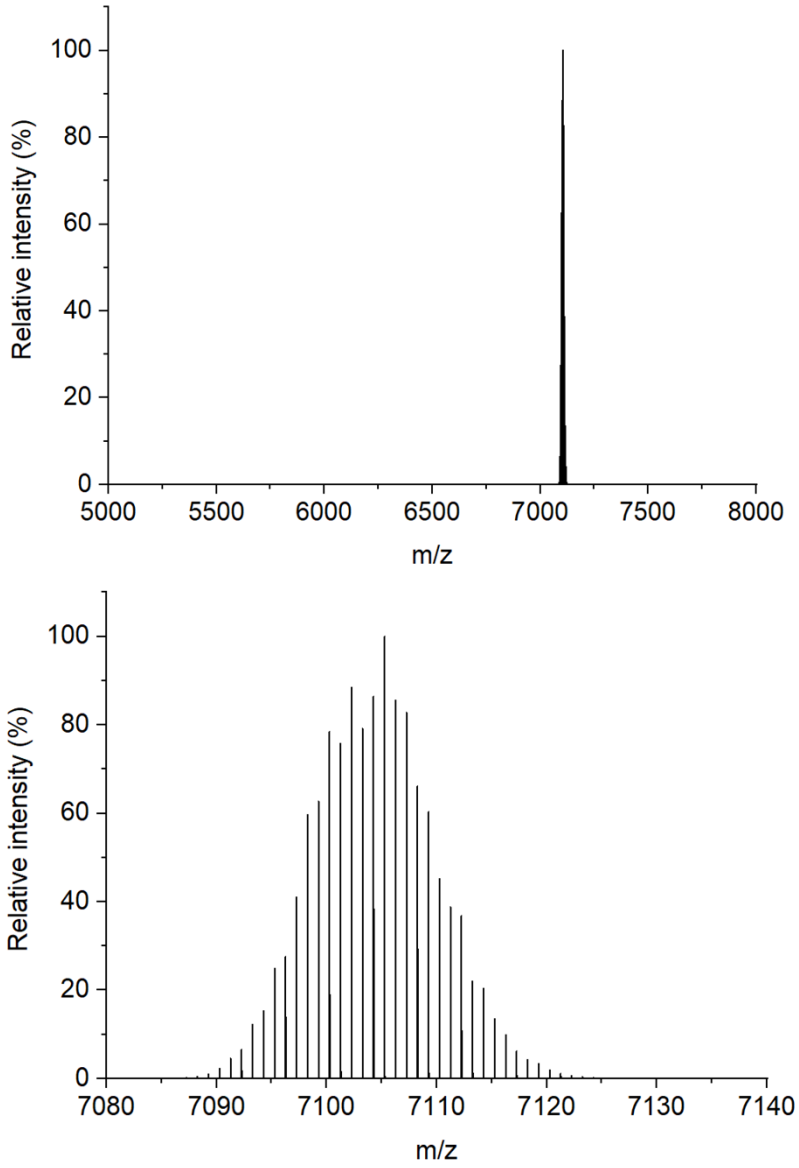

Fig. S13: ESI-MS spectrum of PEI-ZnTPP in Methanol

S2. Photophysical Measurements

S2.1 Singlet Oxygen Quantum Yield Determination

$$\Phi_{\Delta} = \Phi_{Standard}\left(\frac{Peak\ Area\ _{Sample}}{Peak\ Area\ _{Standard}}\right)\left(\frac{Absorbance\ _{Standard}}{Absorbance\ _{Sample}}\right) \quad \textbf{(1)}$$

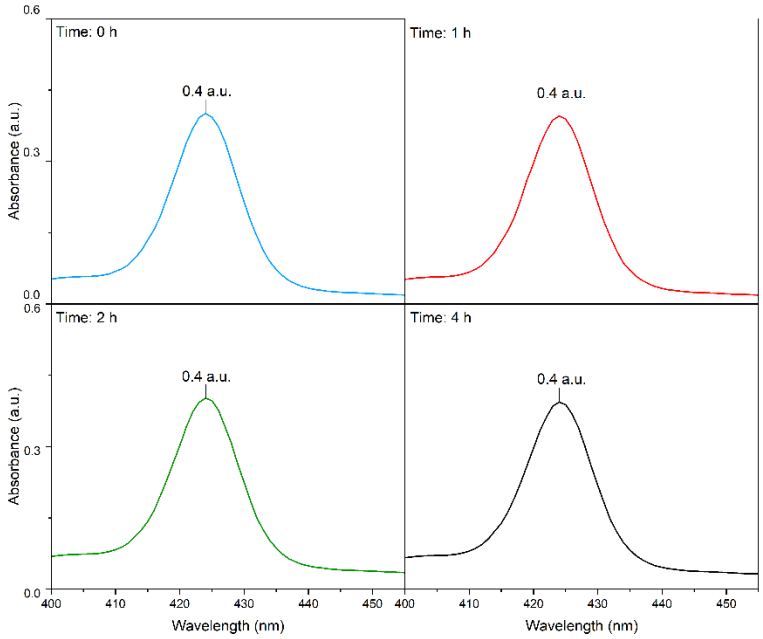

Fig. S14: Absorbance spectra of PEI-ZnTPP recorded in toluene following irradiation at various time intervals using a 590 nm LED corresponding to excitation of the Q-bands.

S2.2 Fluorescence and Transient absorption lifetimes.

Fluorescence lifetimes were fitted using the Fluoracle© software according to **equation 2** below, where B_{1e} refers to the contribution of each lifetime to the fit applied. Transient absorption lifetimes were fitted using the L900 software according to **equation 2**.

$$R(t) = B_{1e}\left(\frac{-t}{\tau_1}\right) + B_{2e}\left(\frac{-t}{\tau_2}\right) + B_{3e}\left(\frac{-t}{\tau_3}\right) + B_{4e}\left(\frac{-t}{\tau_4}\right) \quad \textbf{(2)}$$

S2.3 Steady State Absorption and Emission

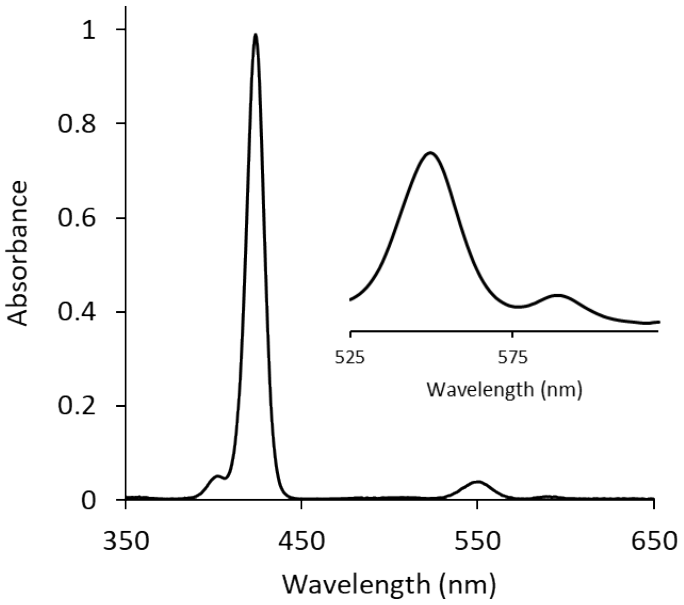

Fig. S15: Absorption spectrum of PEI-ZnTPP in toluene. Insert; expansion of Q (0,0) and Q (0,1) absorptions.

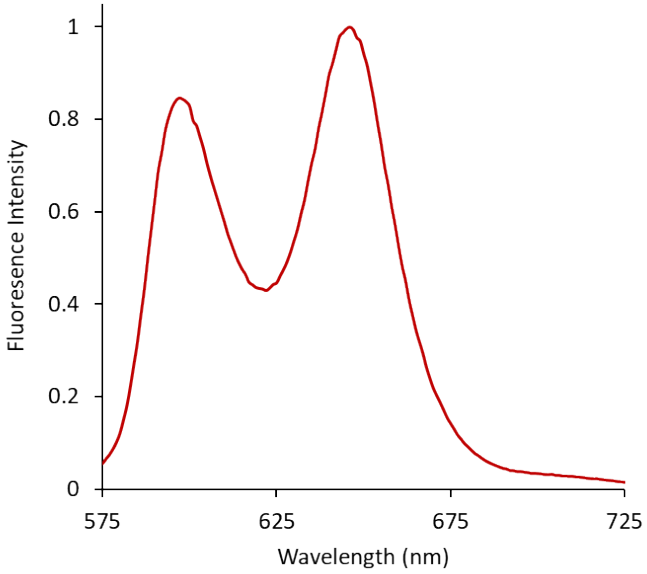

Fig. S16: Emission spectrum of PEI-ZnTPP in toluene

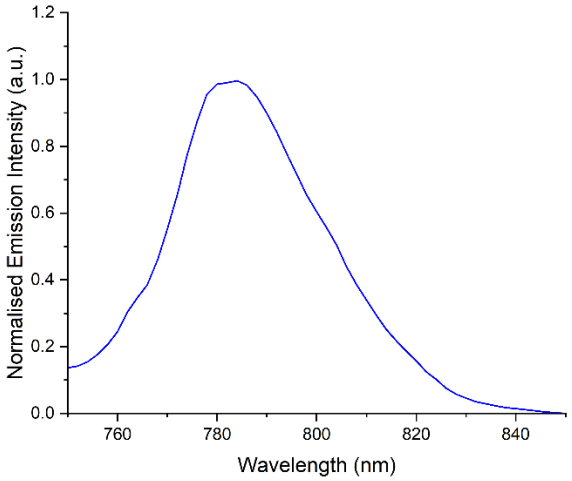

Fig S17: Low temperature (77 K) phosphorescence spectrum of PEI-ZnTPP recorded in a diethyl ether / ethanol / toluene solvent glass (2:1:1 v/v)

Table S2: Absorption and emission parameters for PEI-ZnTPP

Solvent	Absorption				Emission			
	Soret λ_{max} (nm)	FWHM (cm^{-1})	Q (0,1) λ_{max} (nm)	Q (0,0) λ_{max} (nm)	Q (0,0), (0,1) λ_{max} (nm)	Stokes' Shift Q (0,0) (cm^{-1})	τ_F (ns)	Φ_F (%)
Toluene	424	650	549	589	600, 647	311	2	3
THF	424	608	556	596	603, 653	195	2	4
Deposited on glass	442	1878	561	602				

Table S3: Triplet excited state parameters of PEI-ZnTPP

Solvent	0.01 absorbance at 355 nm	0.3 absorbance at 355 nm	Φ_Δ (%)
	τ_T (µs)	τ_T (µs) (% *Contribution)*	
Toluene	197	29 *(0.29)*, 146 *(0.71)*	68
THF	200	28 *(0.26)*, 123 *(0.74)*	63

S2.4 Time Correlated Single Photon Counting

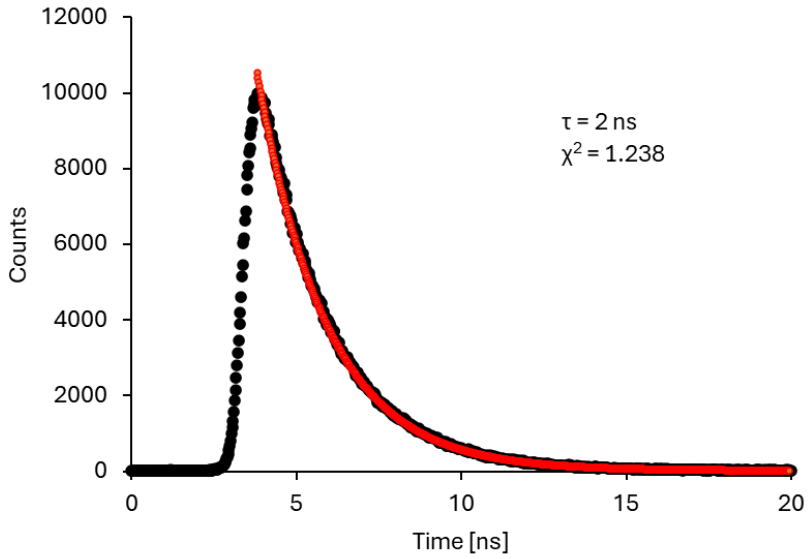

Fig. S18: Fluorescence lifetime decay curve of PEI-ZnTPP in aerated toluene, recorded at 600 nm using 375 nm excitation.

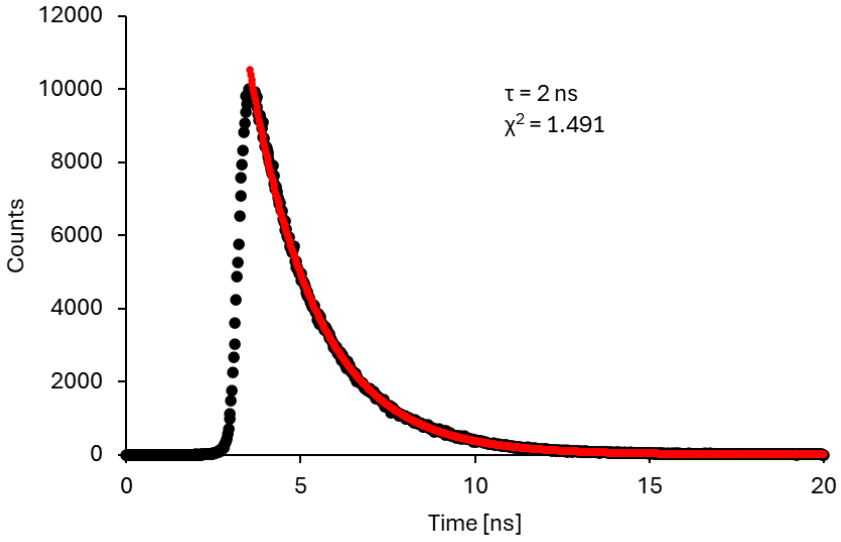

Fig. S19: Fluorescence lifetime decay curve of PEI-ZnTPP in aerated THF, recorded at 603 nm using 375 nm excitation

S2.5 ns-Transient Absorption Spectroscopy

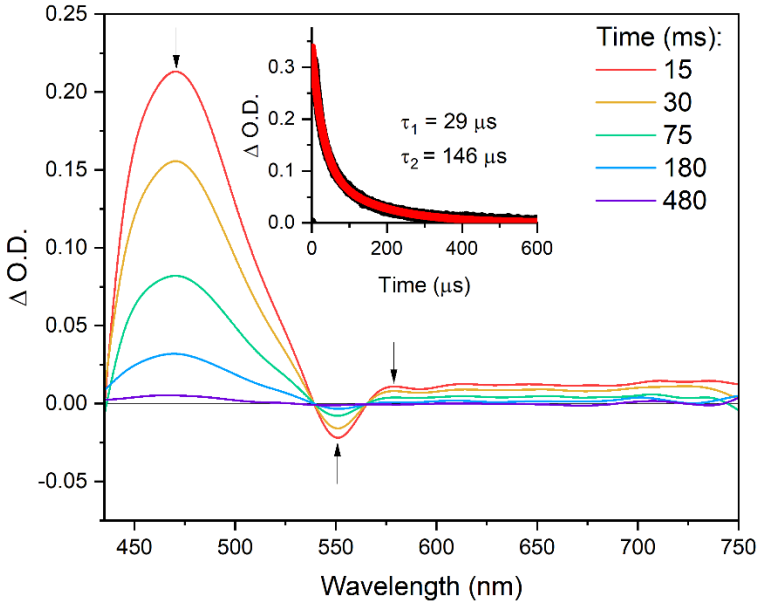

Fig. S20: ns-Transient absorption spectrum of PEI-ZnTPP in toluene (sample absorbance 0.3 a.u. at 355 nm).

Insert lifetime decay curve at 470 nm.

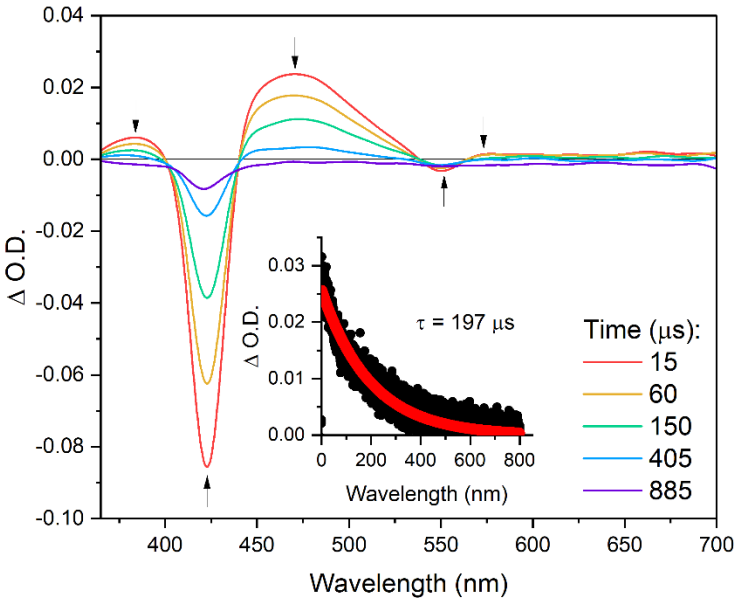

Fig. S21: ns-Transient absorption spectrum of PEI-ZnTPP in toluene (sample absorbance 0.01 a.u. at 355 nm).

Insert lifetime decay curve at 475 nm.

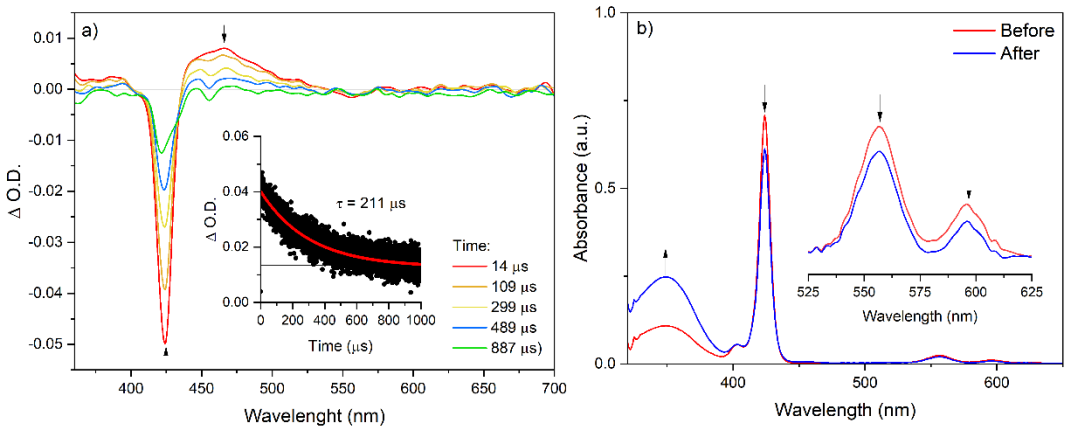

Fig. S22: a) ns-Transient absorption spectrum of PEI-ZnTPP in a 1:1 v/v THF : 0.8 M ascorbic acid(aq) solution, insert kinetic trace for decay of ground state bleach. b) UV-vis absorption spectra of PEI-ZnTPP in a 1:1 v/v THF / 0.8 M ascorbic acid(aq) solution before and after transient absorption spectroscopy.

S3. Photocatalytic Hydrogen Evolution

S3.1 Calculations for Photocatalytic Hydrogen Evolution Rates

Hydrogen evolution was calculated according to **equations** 3, 4 and 5 below, where $n_{H_2}$is the number of moles of H_2 produced (in mmol) in a given experiment, m is the mass of PEI-ZnTPP used (in g) in a given experiment, t it the time (in hours) at a given sampling point, and $n_{PEI-ZnTPP}$ is the moles (in mmol) of PEI-ZnTPP used in a given experiment (as estimated from M_w value obtained from GPC analysis).

$$H_2\ evolution\ mmol\ g^{-1} = \frac{n_{H_2}}{m} \quad \textbf{(3)}$$

$$H_2\ evolution\ mmol\ g^{-1}h^{-1} = \frac{n_{H_2}}{m \times t} \quad \textbf{(4)}$$

$$TON_{H2} = \frac{n_{H_2}}{n_{PEI-ZnTPP}} \quad \textbf{(5)}$$

Table S4: Photocatalytic hydrogen evolution rate of different PEI-ZnTPP loadings of the nanocomposites at different time intervals

Time	Hydrogen Evolution Rate (μmol g^{-1})				
	0.1 mg	**0.2 mg**	**0.4 mg**	**0.8 mg**	**1.2 mg**
1	47,000	20,300	3,300	3,700	800
2	83,500	42,500	8,800	8,300	2,600
4	138,700	84,700	21,300	15,700	5,300

Table S5: Total Hydrogen Evolved in the absence of photocatalytic components

Time	Total Hydrogen Evolved (μmol)					
	PS, TiO_2, Pt^0, SED	**TiO_2,Pt^0, SED**	**PS, TiO_2, SED**	**PT, TiO_2, Pt^0**	**PS, TiO_2, Pt^0, SED (Dark)**	**ZnTPP, TiO_2, Pt^0, SED**
4 h	14	4	0	0	0	4
24 h	59	16	0	0	0	20

S4. Thermodynamic Analysis

Note: In the following section parameters with units of energy are denoted in bold font as ***E***, while those with units of potential are denoted as *E*.

From the 'surface' in **Fig. 5** (main text), the reversible potential, E_{ox}, of the first oxidation of the PEI-ZnTPP immobilised on TiO_2 is 0.365 V vs Fc/Fc+. The optical energy gap between the ground state and excited states, $\boldsymbol{E}_{0,0}$, can be estimated from the intercept wavelength, λ_{int}, between a trend-line drawn tangentially to the lower wavelength (higher energy) edge of the phosphorescence spectrum of Fig. 2d (main text) and the wavelength axis via the well-known wavelength-to-energy expression:

$$\boldsymbol{E}_{0,0} = 1240/\lambda_{int} \qquad (1)$$

A value of λ_{int} = 587 nm 758 nm is so-derived from **Fig.** S17, corresponding to $\boldsymbol{E}_{0,0}$ = 1.64 eV.

The excited state oxidation potential, E_{ox}*, can then be estimated using the expression,[1]

$$E_{ox}^{*} = E_{ox} - E_{0,0} \qquad (2)$$

where $E_{0,0}$ is the numerical value of $\boldsymbol{E}_{0,0}$ expressed in V. This yields a value of E_{ox}* = -1.28 V.

These electrochemical potentials can then be converted to the HOMO and excited state (*) electronic energies (on the vacuum scale) by using the following expressions,

$$\boldsymbol{E}_{HOMO} = -(E_{ox\ (\text{vs Fc/Fc+})} + 4.8)\ \text{eV},\ \boldsymbol{E}^* = -(E_{ox}^{*}\ _{(\text{vs Fc/Fc+})} + 4.8)\ \text{eV} \quad (3),$$

giving $\boldsymbol{E}_{HOMO}$ = -5.2 eV and $\boldsymbol{E}^*$ = -3.5 eV. As we have noted elsewhere,[1] the most accurate additive conversion factor for relating electrochemical potentials (vs. Fc/Fc+) to orbital energies (vs. the vacuum level) is disputed, however in our experience, 4.8 eV is most commonly used in the molecular chemistry literature.

The conduction band edge of the TiO_2 used in this study was determined by the Mott-Schottky approach (see section S5) as ECB ≈ -4.15 eV under the conditions of the photocatalytic experiments (pH 6). .

The oxidation potential of ascorbic acid has been reported as $E_{ox\ AA}$ ≈ -0.34V (vs. $Hg/HgSO_4$) at pH6.[4] Since the reversible potential of the $Hg/HgSO_4$ reference electrode lies at +0.64 V vs. SHE (standard hydrogen electrode),[5] this equates to a value of $E_{ox\ AA}$ ≈ +0.30 V vs SHE. This value can be converted to the vacuum scale using the expression,[6]

$$\boldsymbol{E}_{ox\ AA} = -(E_{ox\ AA\ (\text{vs SHE})} + 4.6)\ \text{eV} \quad (4),$$

delivering a value of -4.9 eV.

Since the excited state of PEI-ZnTPP at $\boldsymbol{E}^*$ = -3.5 eV lies higher than the conduction band edge of TiO_2 ($\boldsymbol{E}_{CB}$ ≈ -4.0 eV) by ca. 0.6 eV, injection of the excited electron from the dye to the TiO_2 nanoparticles is energetically favourable. The thermodynamic potential for proton reduction at pH6 is -0.355 V (vs SHE), equating to -4.25 eV (vs vacuum) so a driving force also exists for onward electron transfer from TiO_2 to the Platinum catalyst to affect hydrogen evolution.

Furthermore, the energy associated with ascorbic acid oxidation ($\boldsymbol{E}_{ox\ AA}$ = -4.9 eV) is greater than that of the PEI-ZnTPP HOMO level ($\boldsymbol{E}_{HOMO}$ = -5.2 eV), implying that an electron can feasibly be transferred from an ascorbic acid molecule to fill the hole in the porphyrin LUMO level created by photoexcitation.

S5. Mott-Schottky Analysis

The value of the conduction band edge, $\boldsymbol{E}_{CB,}$ of the anatase TiO_2 material is an important parameter when considering the thermodynamic feasibility of this photocatalytic system. This can be determined experimentally by electrochemical impedance measurements and their analysis via the Mott-Schottky equation:

$$\frac{1}{C_{SC}^2} = \frac{2}{\varepsilon\varepsilon_0 A^2 e N_D}\left(E - E_{fb} - \frac{kT}{e}\right) \quad (5.1)$$

In equation (5.1), C_{SC} is the semiconductor electrode capacitance, E is the potential, E_{fb} is the flat band potential, A is the electrode surface area, ε is the dielectric constant of the semiconductor material, ε_0 is the permittivity of free space, N_D is the charge carrier density, e is the elementary electric charge, k is the Boltzmann constant, and T is the absolute temperature in Kelvin. The theory and application of the Mott-Schottky equation has been reviewed by us,[1] and others.[5,6] In brief, the equations is valid over a range of potential where depletion of the semiconductor occurs in a region adjacent to the interface with an electrolyte solution. Under these conditions, a plot of $1/C_{SC}^2$ vs. E is predicted to be linear with a slope of $^2/\varepsilon\varepsilon_0 A^2 e N_D$, while the intercept with the E axis equals $E_{fb} + kT/e$. For an n-type semiconductor E_{fb} lies somewhat positive in potential (lower in energy) than the conduction band edge by an amount ΔE.

Mott-Schottky plots for a pristine TiO_2 and PEI-ZnTPP-sensitised TiO_2 are presented in **Fig. S23**, respectively. These measurements were conducted in 0.5 M Na_2SO_4 solution with a measured pH of 6.6. In practice the E axis intercept and slope of Mott-Schottky plots very often show a dependence on measurement frequency[7] and such frequency dispersion is apparent here. Considering **Fig. S23a**, extrapolation of the linear regions of the plots to the E axis yields values of -0.359 and -0.343 V vs. SHE at frequencies of 1.5 and 1.0 kHz, respectively. The flat band potential is obtained by subtracting kT/e (0.025 V at 20°C) from the intercept values to yield E_{fb} values of -0.384 and -0.368 V. For further analysis we take an average E_{fb} value of -0.376 V, which is in good agreement with the literature.[7,8]

To determine the conduction band edge potential, $E_{CB,}$ a value is required for ΔE. Although some reports have used values as high as 0.3 V,[9] a more recent comprehensive study on a photoanodes fabricated from a range of TiO_2 samples has suggested that a more appropriate

value for ΔE lies in the range of 0.1 – 0.15 V. This suggests a value for E_{CB} in the range of -0.476 to -0.526 V. Taking the median value of -0.5 V (vs. SHE), the conduction band edge energy (vs. vacuum) is obtained in an analogous manner to equation (4.4), yielding a value of $\boldsymbol{E}_{CB}$ = -4.1 eV at pH 6.6. The conduction band edge potential of TiO_2 is known to exhibit Nernstian behaviour when in contact with aqueous solutions,[10] implying an energetic shift of + 0.0592 eV per pH unit (at s.t.p.). Therefore, under our photocatalytic conditions (pH 6) a small shift of -0.035 V to $\boldsymbol{E}_{CB}$ = -4.135 ≈ -4.15 eV is required for the purpose of the thermodynamic analysis in section S4.

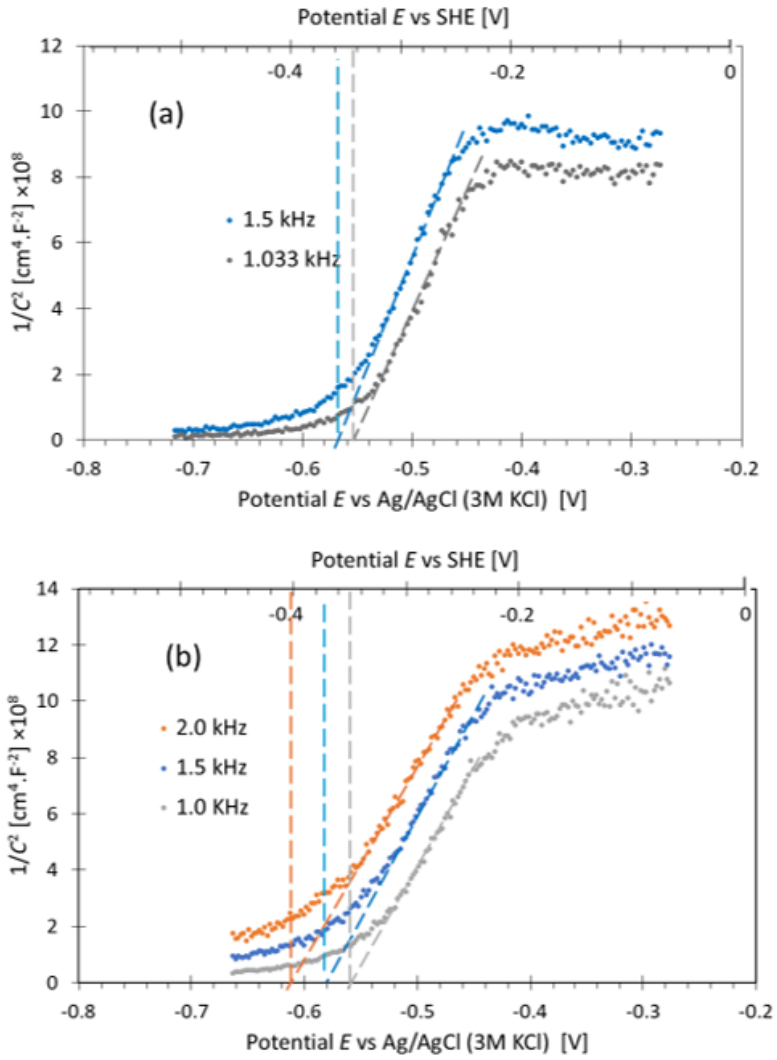

Fig. S23: Mott Schottky plots recorded in 0.5 M Na_2SO_4 for a) TiO_2, and b) PEI-ZnTPP sensitised TiO_2 films on FTO glass electrodes

Charge carrier density, $N_{D,}$ was calculated from the slopes of the Mott-Schottky plots with values obtained in the range of 10^{20} cm^{-3}, where a value of ε = 55 was assumed.[7] Specifically for the data recorded at 1.5 kHz, a value of $N_D = 3.1 \times 10^{20}$ cm^{-3} arose.

In the case of the PEI-ZnTPP sensitised TiO2 electrodes (**Fig. S23b**) the *E* axis intercept values are shifted marginally in the cathodic direction compared to the unfunctionalised sample (TiO_2). For example, at 1.5 kHz, an intercept of -0.375 V (vs. SHE), suggests a value of E_{fb} = -0.400 V, which is 0.015 V lower than the pristine TiO_2 at this frequency. Such a moderate difference probably lies within the margin of error of the Mott-Schottky method and so it can be concluded that sensitisation of the TiO_2 with the PEI-ZnTPP polymer has no significant impact on the conduction band edge potential.

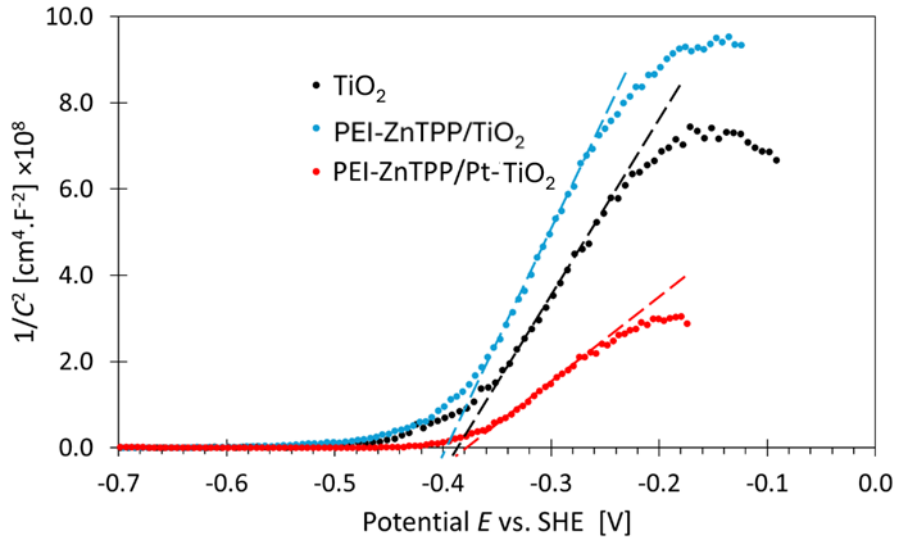

Fig. 24: Mott Schottky plots recorded in 0.5 M Na_2SO_4 (pH 6.6) for TiO_2, PEI-ZnTPP/TiO_2 and PEI-ZnTPP/Pt-TiO2 films drop-cast at room temperature from Nafion/ethanol suspensions. The data has been corrected for the effects of a serial Helmholtz capacitance contribution

Since it is difficult to perform the photo-deposition of platinum nanoparticles onto a TiO_2/FTO film in a manner consistent with the platinization of TiO_2 particles in a suspension, it was chosen to directly fabricate a PEI-ZnTPP/Pt-TiO_2 electrode by casting an ethanolic/Nafion dispersion of a powder of this material onto FTO at room temperature. Unfortunately, it is not possible to apply any heat treatment to electrode configuration due to the low melting point of the PEI-polymer. Accordingly, these films are likely to be inferior to those prepared by conventional methods such as those characterised in **Fig. S23.** Nevertheless, we conducted Mott-Schottky measurements on these, and control TiO_2 and PEI-ZnTPP/TiO_2 electrodes deposited in the same manner. These resulting data was less satisfactory than those presented in **Fig S23**, in that the plots didn't converge towards a zero value in C^{-2} at potentials negative

of the linear sloped region, instead presenting a flat plateau. Such behaviour is consistent with a significant contribution from the Helmholtz layer capacitance, C_H, in series with C_{SC}. To counteract this we applied a protocol[6] to correct for the effect of C_H - the corrected plots at 1.5 kHz are presented in **Fig S24**.

Flat band potentials of -0.410 and -0.423 V (vs NHE) were obtained for the TiO_2 and PEI-ZnTPP/TiO_2 electrodes, respectively. These values are in good agreement with those obtained at 1.5 kHz for the 'more conventional' TiO_2 photoelectrodes in **Figs S23**. The data for the PEI-ZnTPP/Pt-TiO_2 sample exhibits a much shorter linear sloped region, however the E axis intercept occurs adjacent to that of the TiO_2 electrode. This prompts a tentative suggestion that decoration of the TiO_2 surface by platinum nanoparticles at 1 wt% loading does not significantly alter the conduction band position, although more detailed investigations are required to clarify this point.

S6. References

1 J. S. O'Neill, L. Kearney, M. P. Brandon and M. T. Pryce, *Coord. Chem. Rev.*, 2022, **467**, 214599.

2 M. Rueda, A. Aldaz and F. Sanchez-Burgos, *Electrochimica Acta*, 1978, **23**, 419–424.

3 L. Meites, *Handbook of analytical chemistry*, McGraw-Hill, New York, 1963.

4 C. M. Cardona, W. Li, A. E. Kaifer, D. Stockdale and G. C. Bazan, *Adv. Mater.*, 2011, **23**, 2367–2371.

5 K. Gelderman, L. Lee and S. W. Donne, *J. Chem. Educ.*, 2007, **84**, 685.

6 A. Hankin, F. E. Bedoya-Lora, J. C. Alexander, A. Regoutz and G. H. Kelsall, *J. Mater. Chem. A*, 2019, **7**, 26162–26176.

7 S. F. Lee, E. Jimenez-Relinque, I. Martinez and M. Castellote, *Catalysts*, DOI:10.3390/catal13061000.

8 W. Peng, C. Yang and J. Yu, *RSC Adv.*, 2020, **10**, 1181–1190.

9 M. Vafaei and M. R. Mohammadi, *New J. Chem.*, 2017, **41**, 14516–14527.

10 L. Kavan, *J. Solid State Electrochem.*, 2024, **28**, 829–845.